Computers and Concrete, *Vol. 12, No. 5 (2013) 627-650*
DOI: http://dx.doi.org/10.12989/cac.2013.12.5.627

Modelling of the effects of alkali-aggregate reaction in reinforced concrete structures

S. Pietruszczak[*1], R. Ushaksaraei[1] and V. Gocevski[2]

[1]*Department of Civil Engineering, McMaster University, Hamilton, ON, Canada*
[2]*Hydro-Quebec, Montreal, QC, Canada*

(*Received June 13, 2012, Revised May 14, 2013, Accepted July 10, 2013*)

Abstract. This paper deals with application of a non-linear continuum model for reinforced concrete affected by alkali-aggregate reaction (AAR) to analysis of some nuclear structures. The macroscopic behaviour of the material affected by AAR is described by incorporating a homogenization/averaging procedure. The formulation addresses the main stages of the deformation process, i.e., a homogeneous deformation mode as well as that involving localized deformation, associated with formation of macrocracks. The formulation is applied to examine the mechanical behaviour of some reinforced concrete structures in nuclear power facilities located in Quebec (Canada). First, a containment structure is analyzed subjected to 45 years of continuing AAR. Later, an inelastic analysis is carried out for the spent fuel pool taking into account the interaction with the adjacent jointed rock mass foundation. In the latter case, the structure is said to be subjected to continuing AAR that is followed by a seismic event.

Keywords: nuclear powerplant structures; reinforced concrete; alkali-aggregate reaction; chemo-plasticicty

1. Introduction

The integrity of civil structures is essential to maintain continuing operation of nuclear power plants and nuclear facilities. As structures age, the material properties evolve due to environmental influences as well as various chemical processes. The primary objective of the research reported here is to examine the effects of the chemo-mechanical interaction in reinforced concrete structures within nuclear facilities and to assess the corresponding safety-related margins.

The main source of chemically triggered degradation of concrete and reinforced concrete structures is the alkali-aggregate reaction (AAR). The product of the reaction is a gel that imbibes water from the pore fluid and expands triggering a progressive damage of the material. The rate of expansion depends primarily on the available alkali content of concrete. Other factors influencing the kinetics of the reaction are the relative humidity, temperature and the confining stress.

In the last few decades a significant amount of research has been devoted to physicochemical aspects of AAR in *plain* concrete and its influence on the behaviour of existing structures (c.f. Can. J. Civil Eng. 2000, Proceedings of ICAAR 2004, Proceedings of ICAAR 2008). In parallel

∗Corresponding author, Professor, E-mail: pietrusz@mcmaster.ca

 ISSN: 1598-8198 (Print), 1598-818X (Online)

with these investigations, a number of experimental studies have been carried out examining the kinetics of the reaction and the associated degradation of mechanical properties of the material. An outstanding contribution in this area is a comprehensive experimental research by Larive (1998). More recent work on the reaction kinetics includes the studies dealing with the influence of alkali concentration (Rivard *et al.* 2007), effects of humidity (Poyet *et al.* 2006), applied stress (Multon *et al.* 2008), reactive aggregate size distribution (Poyet *et al.* 2007) as well as the use of powder glass/glass as a filler/fine aggregate (Dhir *et al.* 2009). At the same time, the research on development of constitutive models describing the chemo-mechanical interaction has been somewhat limited. More general continuum approaches, involving the framework of chemo-plasticity/elasticity, started to appear in the mid 1990 (Pietruszczak 1996, Capra and Bournazel 1998). Later, several derivative concepts were proposed that included both the continuum models (e.g., Ulm *et al.* 2000, Steffens *et al.* 2003, Multon and Toutlemonde 2006, Saouma and Perotti 2006, Grimal *et al.* 2008) as well as micromechanical descriptions of AAR-induced deformation (cf. Bazant and Steffens 2000, Bazant *et al.* 2000). It needs to be pointed out, however, that the recent developments deal with plain concrete only and are, in general, inadequate in terms of modelling of localized deformation, which is intrinsic in the type of problems considered here. Furthermore, there have only been a few isolated attempts to perform large-scale simulations that involved the actual engineering structures. Most of these attempts (e.g., Saouma and Perotti 2006, Sellier *et al.* 2009) dealt primarily with the assessment of the influence of concrete expansion on the structural integrity, without accounting for the reaction-dependent evolution of material properties and a rather simplistic description of the onset and propagation of localized damage, particularly in compression regime.

The present work follows the general approach proposed in an article by Pietruszczak (1996), albeit with significant revisions that pertain to the incorporation of heavy reinforcement and the description of the reaction kinetics. The model is a direct extension of the framework presented earlier by Pietruszczak and Winnicki (2003), in which the reinforced concrete is considered as a composite medium comprising concrete matrix and two orthogonal families of reinforcement. The latter formulation has been recently generalized (Winnicki and Pietruszczak 2008) to incorporate the chemo-mechanical interaction associated with continuing AAR.

The mechanical behaviour of reinforced concrete affected by AAR is described by employing a non-linear continuum theory that incorporates a chemo-mechanical coupling. In general, the most efficient way of analysing heavily reinforced large concrete structures is to use a homogenization technique. In this approach, the reinforced concrete is considered as a composite medium comprising the concrete matrix and a set of families of reinforcement. The overall macroscopic behaviour is then defined by employing suitable averaging procedures. In the framework employed here, the concrete is assumed to be strengthened with two orthogonal sets of reinforcing steel bars. The formulation addresses the main stages of the deformation process, i.e. a homogeneous deformation mode as well as that involving localized deformation, associated with formation of macrocracks. In the former case, i.e. prior to cracking, the problem is formulated by invoking a volume averaging procedure. After the onset of localization, the representative volume incorporates the fractured zone and the adjacent 'intact' material, both reinforced with steel bars. In this case, the stiffness of the reinforcement network and the criterion of yielding are both assessed in a discrete sense, by considering the bending characteristics of individual bars rigidly embedded in the adjacent intact material. The concrete itself is assumed to suffer from continuing alkali-aggregate reaction. The mathematical description of the effects of the reaction is based on chemo-plasticity and invokes the assumption that the formation of expansive phases results in

progressive degradation of both strength and deformation properties of the material.

In what follows, the governing constitutive relations, which have been incorporated in a finite element code, are first reviewed. Later, the results of numerical studies are presented. First, the mechanical response of a containment structure of a nuclear facility located near the community of Trois-Rivières in Québec is examined. Subsequently, an inelastic analysis is carried out for a spent fuel exchange pool subjected to continuing AAR followed by a seismic event typical for the region. The latter analysis takes into account the interaction with the adjacent rock mass. In that part, a new constitutive framework for describing the inelastic response of the existing jointed rock foundation is presented first. Later, an extensive discussion on the results of numerical simulations is provided.

2. Mathematical formulation

As mentioned earlier, the specific form of the constitutive relation for describing the AAR-affected reinforced concrete is that proposed in the recent article by Winnicki and Pietruszczak (2008). In this approach, the material is treated as a composite medium comprising the AAR-affected concrete matrix (*m*) and two orthogonal families of reinforcement (sets 1 and 2, respectively).

For concrete matrix, the formulation incorporates a scalar parameter ζ which is a measure of the continuing reaction and is defined as

$$\zeta(t)=\frac{\in(t)}{\bar{\in}}; \qquad \bar{\in}=\in(t\to\infty) \tag{1}$$

Here, $\in(t)$ is the volumetric expansion of concrete and $\bar{\in}$ is a material parameter that defines the maximum value of $\in$, for a given alkali content, in the stress free state. The evolution law is assumed in a simple linear form

$$\dot{\zeta}=\gamma(\bar{\zeta}-\zeta) \quad \text{for } t\geq t_0 \;\Rightarrow\; \zeta=\bar{\zeta}(1-e^{-\gamma\langle t-t_0\rangle}); \qquad \zeta=0 \quad \text{for} \quad t<t_0 \tag{2}$$

where $\bar{\zeta}$ can be interpreted as a value of the state variable ζ associated with the chemical equilibrium, γ is a material constant describing rate of the reaction, and t_0 is the initiation time. The closed form integration for ζ in Eq. (2) is based on a constant value of $\bar{\zeta}$, where $\langle\ldots\rangle$ are Macauley brackets. The value of $\bar{\zeta}$ depends, in general, on the confining pressure, temperature and relative humidity.

The formulation of the constitutive relation that governs the chemo-mechanical interaction follows the framework established in an earlier article by Pietruszczak and Gocevski (2002). In the *elastoplastic* range, the additivity of elastic and plastic strain rates leads to

$$\dot{\boldsymbol{\varepsilon}}=[C^e]\dot{\boldsymbol{\sigma}}+\mathbf{b}\dot{\zeta}+\dot{\boldsymbol{\varepsilon}}^p \;\Rightarrow\; \dot{\boldsymbol{\sigma}}=[D^e](\dot{\boldsymbol{\varepsilon}}-\dot{\boldsymbol{\varepsilon}}^p-\mathbf{b}\dot{\zeta}); \qquad \mathbf{b}=\frac{\partial}{\partial\zeta}[C^e]\boldsymbol{\sigma}+\frac{1}{3}\bar{\in}\boldsymbol{\delta} \tag{3}$$

in which $[D^e]=[C^e]^{-1}$, where $[C^e]$ is the elastic compliance. In order to define the plastic strain rates, the functional form of the yield criterion f=0 is assumed to be affected by the progress in the reaction, i.e. $f=f(\boldsymbol{\sigma},\boldsymbol{\varepsilon}^p,\zeta)$. Following a standard plasticity procedure, the constitutive relation can be obtained as

$$\dot{\boldsymbol{\varepsilon}} = [C]\dot{\boldsymbol{\sigma}} + \boldsymbol{\Gamma}\dot{\zeta}; \quad \boldsymbol{\Gamma} = \mathbf{b} + \frac{1}{H}\frac{\partial f}{\partial \zeta}\frac{\partial Q}{\partial \boldsymbol{\sigma}} = \frac{\partial}{\partial \zeta}[C^e]\boldsymbol{\sigma} + \frac{1}{H}\frac{\partial f}{\partial \zeta}\frac{\partial Q}{\partial \boldsymbol{\sigma}} + \frac{1}{3}\Subset \boldsymbol{\delta} \tag{4}$$

where Q is the plastic potential function and

$$[C] = [C^e] + \frac{1}{H}\frac{\partial Q}{\partial \boldsymbol{\sigma}}\left(\frac{\partial f}{\partial \boldsymbol{\sigma}}\right)^T; \quad H = -\left(\frac{\partial f}{\partial \boldsymbol{\varepsilon}^p}\right)^T \frac{\partial Q}{\partial \boldsymbol{\sigma}} \tag{5}$$

In the equations above, [C] is the elastoplastic compliance operator, H is the plastic hardening modulus and $\boldsymbol{\delta}$ is the Kronecker's delta.

For reinforced concrete, the problem is formulated in two stages (Pietruszczak and Winnicki 2003). Stage I deals with the homogeneous deformation mode prior to cracking of the concrete matrix, whereas stage II involves a localized deformation associated with formation of macrocracks.

2.1 Stage I (prior to cracking)

The problem is referred to the frame of reference $\mathbf{x}^*$, such that x_2^* and x_3^* are along the axes of reinforcement. The average macroscopic stress/strain rates for the composite body are defined through the volume averaging procedure (Hill 1963), i.e.

$$\dot{\boldsymbol{\sigma}}^* = \eta_1\dot{\boldsymbol{\sigma}}_1^* + \eta_2\dot{\boldsymbol{\sigma}}_2^* + (1-\eta_1-\eta_2)\dot{\boldsymbol{\sigma}}_m^*; \quad \dot{\boldsymbol{\varepsilon}}^* = \eta_1\dot{\boldsymbol{\varepsilon}}_1^* + \eta_2\dot{\boldsymbol{\varepsilon}}_2^* + (1-\eta_1-\eta_2)\dot{\boldsymbol{\varepsilon}}_m^* \tag{6}$$

where η_1 and η_2 represent the volume fractions of the respective sets of reinforcement, whereas $\dot{\boldsymbol{\sigma}}_k^*, \dot{\boldsymbol{\varepsilon}}_k^*$ $(k = 1, 2, m)$ are the averages of stress/strain rates in the constituents involved. Both these local fields are assumed to be homogeneous within themselves, so that

$$\dot{\boldsymbol{\varepsilon}}_1^* = [C_1^*]\dot{\boldsymbol{\sigma}}_1^*; \quad \dot{\boldsymbol{\varepsilon}}_2^* = [C_2^*]\dot{\boldsymbol{\sigma}}_2^*; \quad \dot{\boldsymbol{\varepsilon}}_m^* = [C_m^*]\dot{\boldsymbol{\sigma}}_m^* + \boldsymbol{\Gamma}^*\dot{\zeta} \tag{7}$$

where [C^*]'s are the compliance operators. The reinforcing steel is considered to be an elastic–perfectly plastic von Mises material obeying an associated flow rule, while the behaviour of concrete matrix is governed by Eq.(4).

The local stress rate averages can be related to the overall macroscopic measure $\dot{\boldsymbol{\sigma}}^*$ viz.

$$\dot{\boldsymbol{\sigma}}_1^* = [B_1]\dot{\boldsymbol{\sigma}}^* + [\bar{B}_1]\boldsymbol{\Gamma}^*\dot{\zeta}; \quad \dot{\boldsymbol{\sigma}}_2^* = [B_2]\dot{\boldsymbol{\sigma}}^* + [\bar{B}_2]\boldsymbol{\Gamma}^*\dot{\zeta}; \quad \dot{\boldsymbol{\sigma}}_m^* = [B_m]\dot{\boldsymbol{\sigma}}^* + [\bar{B}_m]\boldsymbol{\Gamma}^*\dot{\zeta} \tag{8}$$

The details on the specification of operators [B] and [$\bar{B}$], based on imposing some explicit kinematic constraints, are provided in the original reference.

Combining the above equations, the macroscopic constitutive relation can be established as

$$\begin{aligned} &\dot{\boldsymbol{\varepsilon}}^* = [C^*]\dot{\boldsymbol{\sigma}}^* + [\bar{C}^*]\boldsymbol{\Gamma}^*\dot{\zeta}; \quad [C^*] = \{\eta_1[C_1^*][B_1] + \eta_2[C_2^*][B_2] + (1-\eta_1-\eta_2)[C_m^*][B_m]\}; \\ &\qquad [\bar{C}^*] = \{\eta_1[C_1^*][\bar{B}_1] + \eta_2[C_2^*][\bar{B}_2] + (1-\eta_1-\eta_2)([C_m^*][\bar{B}_m] + [I])\} \end{aligned} \tag{9}$$

Apparently, the macroscopic stress/strain rates can be transformed to an arbitrarily chosen global Cartesian system by following the standard transformation rules.

The above equation defines the response of the composite prior to formation of macrocracks in the concrete matrix. In reinforced concrete structures, the cracking is typically associated with the

tensile stress regime. Once a macrocrack forms, the formulation of the problem follows the procedure outlined below.

2.2 Stage II (after formation of a macrocrack)

The representative volume of the material comprises now the 'intact' reinforced concrete intercepted by a macrocrack of a given orientation $\boldsymbol{n}$. The latter represents a composite medium within itself as it consists of a zone of fractured concrete reinforced with steel bars. A volume averaging procedure can be used again for specifying the macroscopic rates, i.e.

$$\dot{\boldsymbol{\sigma}} = \mu_i \dot{\boldsymbol{\sigma}}_i + \mu_f \dot{\boldsymbol{\sigma}}_f ; \qquad \dot{\boldsymbol{\varepsilon}} = \mu_i \dot{\boldsymbol{\varepsilon}}_i + \mu_f \dot{\boldsymbol{\varepsilon}}_f \tag{10}$$

Here, i refers to the intact material outside the localization zone, f denotes the material in the fractured zone and μ's represent the corresponding volume fractions. All quantities are referred to the global coordinate system $\boldsymbol{x}$. The strain rate in the fractured zone can be expressed in terms of velocity discontinuities $\dot{\boldsymbol{g}}$. Thus, the constitutive relations governing the behaviour of the intact material and the interface are as follows

$$\dot{\boldsymbol{\varepsilon}}_i = [C]\dot{\boldsymbol{\sigma}}_i + [\bar{C}]\boldsymbol{\Gamma}\dot{\zeta} ; \qquad \dot{\boldsymbol{\varepsilon}}_f = \frac{1}{h}[N]\dot{\boldsymbol{g}} ; \qquad \dot{\boldsymbol{g}} = [K]^{-1}\dot{\boldsymbol{t}} ; \qquad \dot{\boldsymbol{t}} = [N]^T \dot{\boldsymbol{\sigma}}_i \tag{11}$$

where $[K]$ denotes the stiffness of the fractured zone, $\boldsymbol{t}$ is the traction vector, and h denotes the thickness of the cracked zone. Noting that $\mu_f \ll \mu_i$ and employing Eq. (10), the average macroscopic response of the composite can be defined as

$$\dot{\boldsymbol{\varepsilon}} \approx ([C] + \mu[N][K]^{-1}[N]^T)\dot{\boldsymbol{\sigma}} + [\bar{C}]\boldsymbol{\Gamma}\dot{\zeta} \tag{12}$$

Here, $\mu = \mu_f / h$ represents the ratio of the area of the fractured zone to the representative volume of the sample. Thus μ is, in fact, independent of h.

The approach outlined above requires an assessment of the mechanical properties of the fractured zone, viz. operator $[K]$. This zone is composed of the damaged concrete and the network of reinforcement. The details on the description of mechanical characteristics are provided in the article by Pietruszczak and Winnicki (2003).

The particular formulation employed here to describe the nonlinear behaviour of concrete matrix is similar to that outlined by Pietruszczak *et al*. (1988). It invokes a non-associated flow rule and the yield surface is expressed in a functional form

$$f = \bar{\sigma} - \alpha(\zeta)\beta(\xi)k(\theta)\bar{\sigma}_c = 0; \quad \dot{\xi} \propto (\frac{1}{2}\dot{e}^p_{ij}\dot{e}^p_{ij})^{1/2}; \quad \bar{\sigma}_c = \frac{-a_1 + \sqrt{a_1^2 + 4a_2(a_3 + I/f_c)}}{2a_2} f_c \tag{13}$$

In the equations above a's are material constants normalized with respect to axial compressive strength (f_c); $I = -I_1, \bar{\sigma} = (J_2)^{1/2}, \theta = \frac{1}{3}\sin^{-1}(3\sqrt{3}J_3 / 2\bar{\sigma}^3)$, where I_1 and (J_2, J_3) are the basic invariants of the stress tensor and stress deviator, respectively. The degradation of strength properties is governed here by the variable $\alpha(\zeta)$. In general, all degradation functions, for elastic moduli as well as strength, are assumed in a simple linear form

$$E = E_0\left[1-(1-B_1)\zeta\right]; \qquad \nu = \nu_0\left[1-(1-B_2)\zeta\right]; \qquad \alpha = 1-(1-B_3)\zeta \tag{14}$$

where *B*'s are material parameters. Finally, there is evidence that a high confining pressure slows down the reaction (Multon *et al*. 2006, Saouma and Perotti 2006). Therefore, for a given alkali content and humidity, the parameter $\bar{\zeta}$ is taken as a function of the confining pressure, and its evolution is described via an exponential form

$$\bar{\zeta} = e^{-A_1\sqrt{\frac{\langle -tr(\boldsymbol{\sigma})\rangle}{3f_c}}} \tag{15}$$

where A_1 is a material constant. Note that the dependence of $\bar{\zeta}$ on the temperature and humidity is explicitly addressed in Pietruszczak and Gocevski (2002).

3. Numerical analysis

In this section, the results of some numerical simulations are provided. In particular, the framework described in Section 2 is applied to examine the mechanical behaviour of some structural elements within the Gentilly-2 (G2) nuclear powerplant, situated near the community of Trois-Rivières in Quebec. The concrete of G2 is known to have been suffering from continuing AAR. The aggregate in this concrete is a siliceous limestone from the region of Trois-Rivières. It is recognized as highly to extremely reactive according to the criteria established by CSA (Canadian Standards Association). The latter incorporate a combination of test procedures that include a petrographic examination, immersion tests on drilled cores as well as the concrete prism tests.

The surface cracking of concrete at G2 powerplant started during the construction stage and gradually worsens over time due to the effects of AAR and the continuing thermal cycles typical for the Canadian climate. The propagation of cracks (now penetrating, on average, about 100mm into the walls) and the changes of pre-stressing over time are continuously influencing the structural behaviour. The main issue, after 27 years of operation, is the ultimate pressure capacity (UPC) and the air tightness of the reinforced concrete envelope, which depend mainly on the losses/gains of post-tensioning forces. The latter are due to AAR-effects as well as the damage that can be attributed to shrinkage and aging of concrete caused by freeze-thaw cycles (Gocevski 2003, 2010). In what follows, the results of numerical simulations aimed at evaluation of the extent of damage in the containment building subjected to own weight, post-tensioning and AAR, are presented first. Then, the results of FE analysis of the spent fuel pool under self-weight, 50 years of continuing AAR, and seismic load typical for the region are discussed.

3.1 Containment structure

The evolution of damage within the concrete walls of the containment structure of G2 is examined first. The ultimate pressure capacity is directly affected by the formation and a slow propagation of micro and macrocracks. Therefore, it is important to predict the time-history of their occurrence in order to assess the need for implementing some remedial measures to maintain the air tightness of the building, as imposed under the requirements of the Canadian Commission of Nuclear Safety (CCNS). The structure, shown in Fig. 1, was analyzed using the constitutive model for AAR-affected reinforced concrete, as discussed earlier. The analysis was conducted using the primary set of material properties specified in Table 1. In general, the problem of

identification of parameters in the context of existing old-aged concrete affected by AAR, is addressed in a recent paper by Herrador *et al*. (2008). Here, the key strength/deformation parameters and their degradation rates were obtained from core-drilled samples extracted from different locations within the structure. At the same time, the parameters governing the kinetics of expansion were estimated directly from in-situ measurements. The following values were assumed

$$\bar{\in}=0.01704\ ;\ \gamma=0.092\ (1/day)\ ;\ B_1=0.7\ ;\ B_2=0\ ;\ B_3=0.9\ ;\ A_1=8.3$$

Note that during the construction of the reactor building 139 vibrating wire extensometer were installed in three directions (i.e., horizontal tangential, horizontal radial and vertical) in the concrete walls (through the entire height), the dome and the base slab of the concrete envelope. Beginning from 1979, regular readings of the instruments were collected and reported annually (Gocevski 2003).

The temperature in the reactor building varies from 25°C at the base slab up to 40°C near the dome. The relative humidity in the building varies from 25% to 70%. The outside temperature for the region of Trois-Rivières, where the power plant is located, varies from -25°C to +23°C during winter and summer, respectively, while the corresponding ambient relative humidity varies from 25% to 100%. Given this information, both the heat and humidity transfer analyses were conducted within the concrete of the reactor building envelope. The results were used to define approx. 20 areas (locations) having different free expansion rate for the AAR affected concrete. Fig. 1 shows the discretization of the structure. The actual numerical model, as shown in the bottom figure, distinguishes between the regions experiencing different kinetics of the reaction.

The perimeter wall has circumferential post-tensioning tendons and vertical tendons while the upper dome consists of three layers of superimposed tendons, the latter placed in such a way that the tendons form spherical equilateral triangles. The equivalent initial compressive stresses in the concrete sections were evaluated based on spacing of the cables in the structural elements. The average values were estimated as: 10.7 MPa for the two perpendicular principal components in spherical plane of the superior dome, 5.9 MPa for circumferential and 3.5 MPa for vertical direction of the wall, and finally 4.4 MPa and 2.3 MPa for the inferior and superior part of the ring beam, respectively.

The results describing the response of the structure under own weight, post-tensioning, and the continuing AAR are shown in Figs. 2-4. Fig. 2 presents the distribution of damage factor, $ß$, Eq. (13), after 12, 17, and 32 years of ongoing reaction. Note that the values of $ß > 1$ are indicative

Table 1 Material properties

Concrete elastic properties	E = 34.5 GPa; υ = 0.2
Concrete compressive strength	
(initial @ 28 days)	f_{co} = 35 MPa
(measured - 2010)	f_{c2010} = 52 MPa
(estimated – 2035)	f_{c2035} = 58 MPa
Concrete tensile strength	
(initial @ 28 days)	f_{to} = 2.72 MPa
(measured - 2010)	f_{c2010} = 2.0 MPa
(estimated – 2035)	f_{c2035} = 1.5 MPa
Post-tensioning (estimated-2035)	1.06 x (initial post-tensioning)
Reinforcement	E = 200 GPa; υ = 0.3; σ_y = 400 MPa

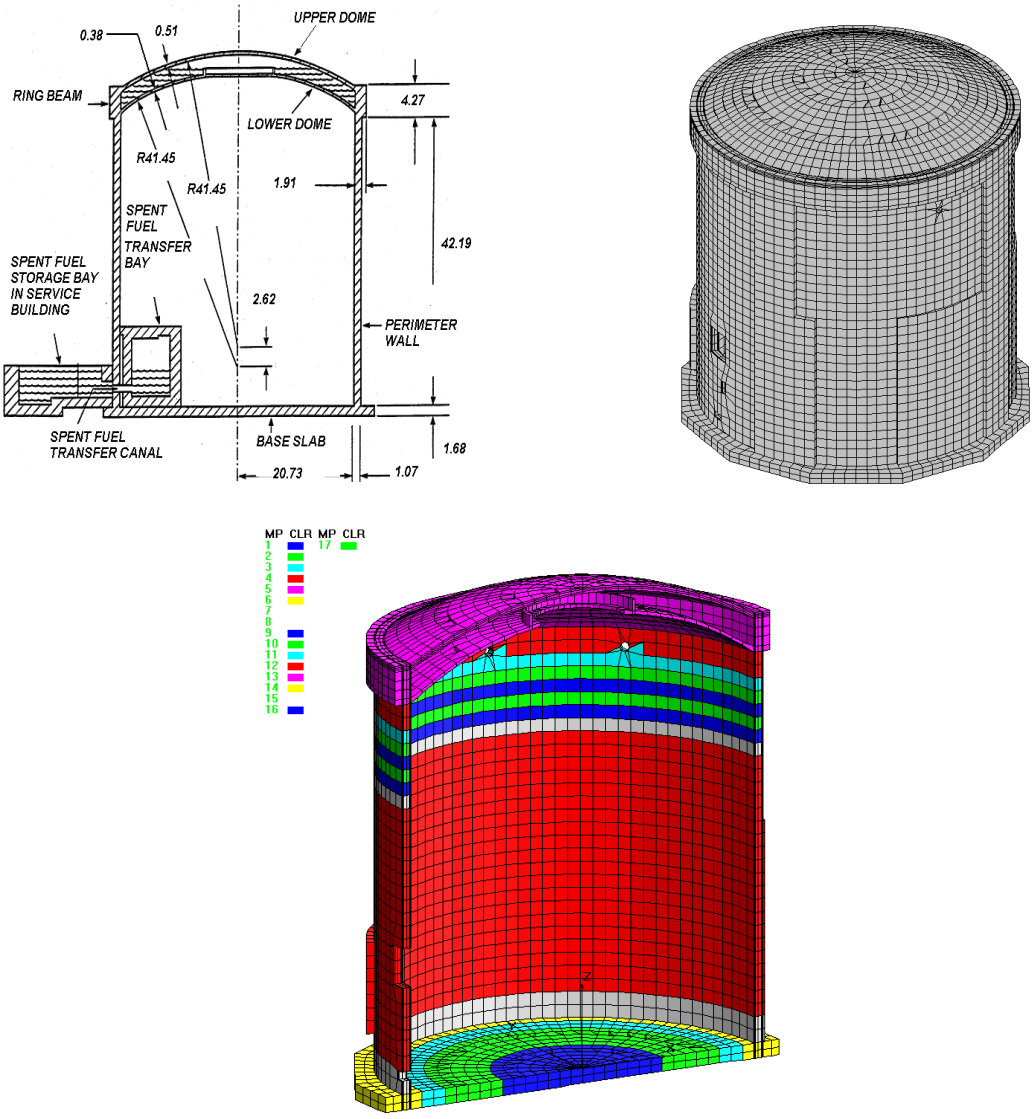

Fig. 1 Containment building; cross-section and the discretization of the structure (top); regions with different reaction kinetics (bottom)

of an unstable response associated with formation of macrocracks. The evolution of the distribution of damage factor in the horizontal section of the wall opposite the opening is shown in Fig. 3. The results indicate the presence of a damage zone, which at some locations penetrates through the entire thickness of the wall. However, the macrocracks are not more than 0.15mm wide. Fig. 4 shows the distribution of damage factor β at the connection of perimeter wall with the base slab. In general, the extent of damage after 45 years of continuing AAR is not very significant. The containment is structurally sound and only minor refurbishment from inside the building may be required to ensure adequate air tightness.

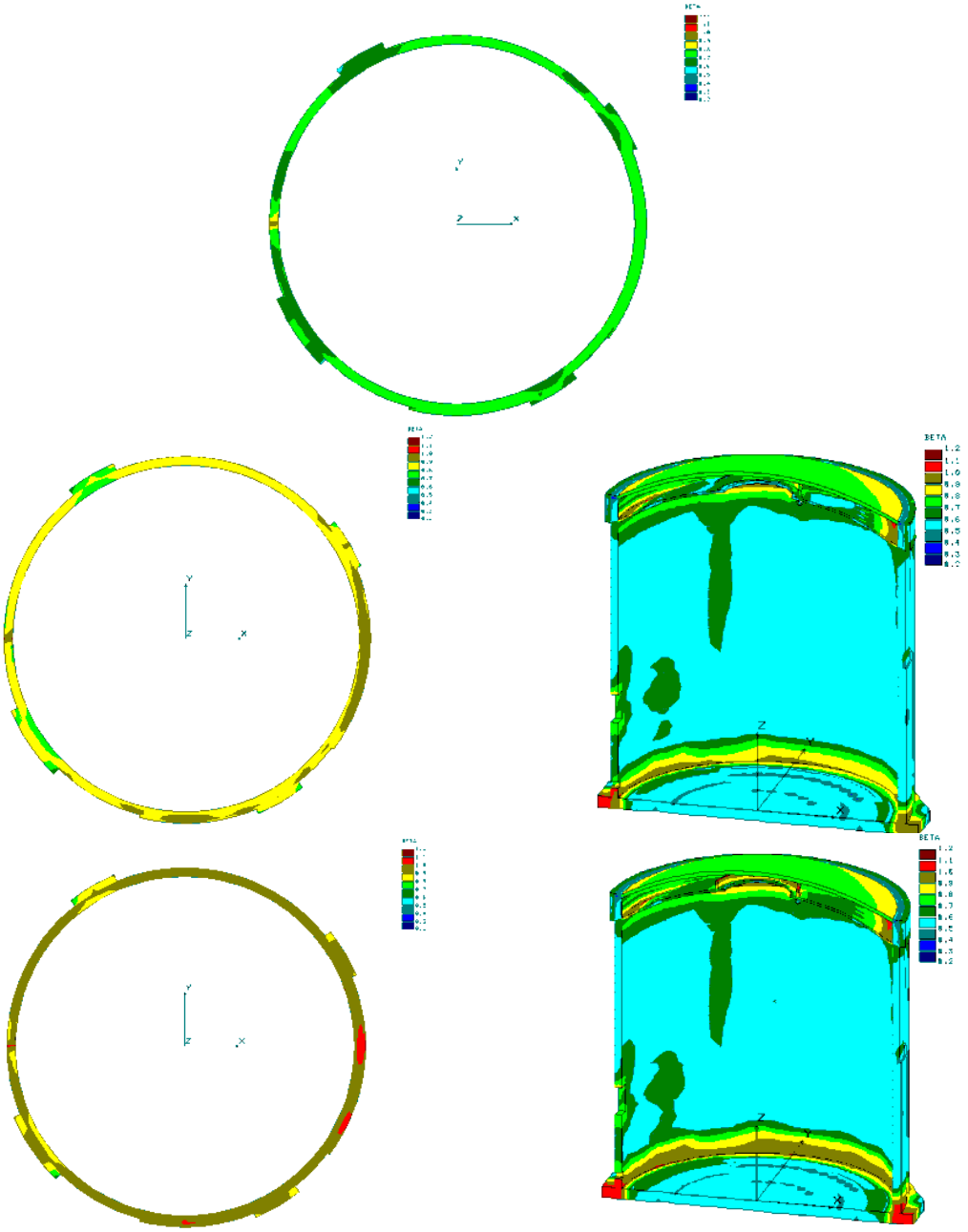

Fig. 2 Distribution of damage factor, β, due to work load and the AAR continuing for 12 years (onset of micro-cracking), 17 years, and 32 years (from top to bottom, respectively); horizontal section at z = 1.41m

In order to verify the quantitative abilities of the framework, some aspects of the results were compared with the actual in-situ measurements. Fig. 5 shows the time histories of vertical and horizontal strains at some different locations of the build-in extensometers. The numerical estimates are clearly within the linear range of approximation.

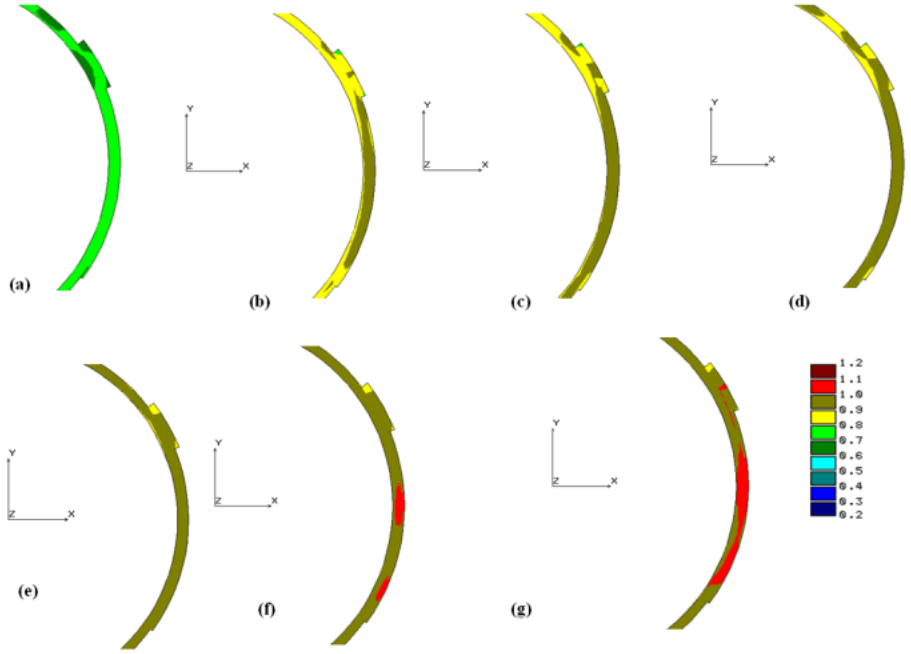

Fig. 3 Distribution of damage factor, β, due to work load and the AAR continuing for (a) 12, (b) 17, (c)20 (d) 22, (e) 25, (f) 32**,** (g) 35 years; horizontal section at z = 1.41m. Detail of the wall opposite of the opening

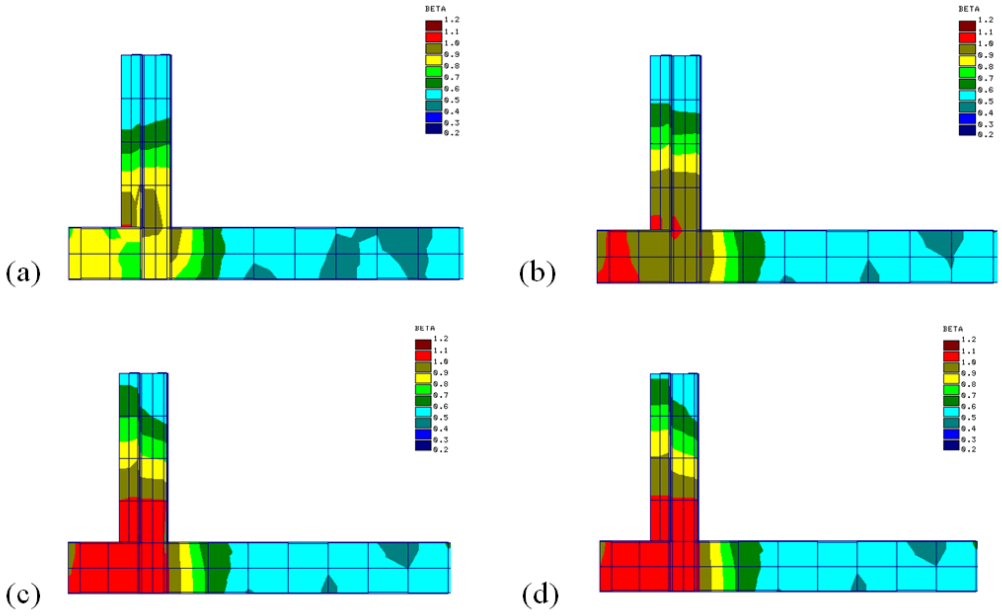

Fig. 4 Distribution of damage factor β at the connection of perimeter wall with base slab due to work load and AAR continuing for : (a) 20 , (b) 30 , (c) 40 , (d) 45 years

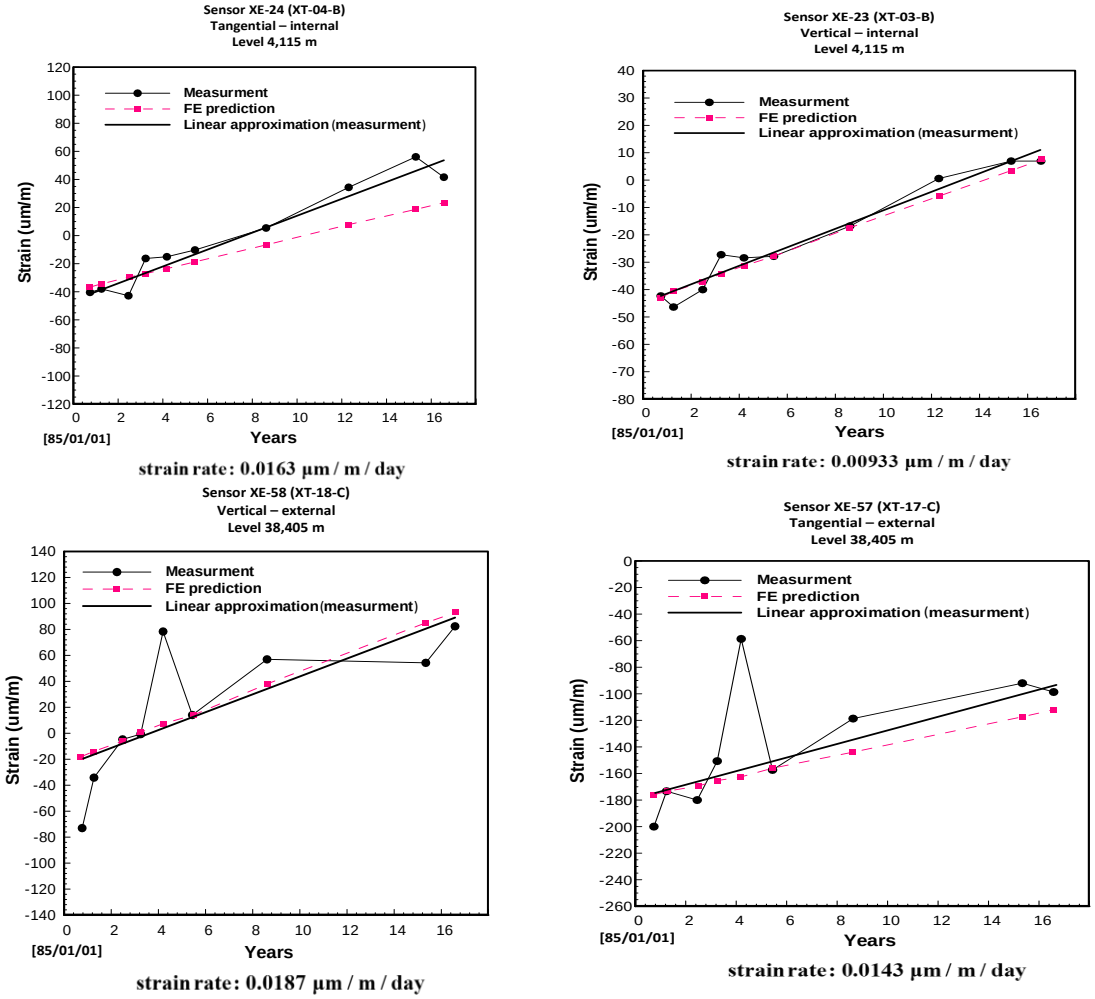

Fig. 5 Numerical predictions vs. measurements for time history of vertical and horizontal strains at the interior/exterior of the circumferential wall of containment building, (a) at elevation 4.115 m and (b) at elevation 38.405 m, 203 degrees North.

3.2 Spent fuel pool

In this section the results of FE analysis of reinforced concrete structure of the spent fuel storage pool of G-2 generating station, subjected to 50 years of continuing AAR and the seismic load are presented. The analysis takes into account the interaction of the structure with the jointed rock mass foundation. In what follows, the constitutive relation for describing the inelastic response of the foundation is discussed first, followed by presentation of the numerical results.

(i) Modeling of jointed rock mass

Fig. 6 shows a schematic diagram of a representative volume of the material, which consists of intact rock intercepted by two families of joints with given orientations, $n_i^{(1)}$ and $n_i^{(2)}$. The

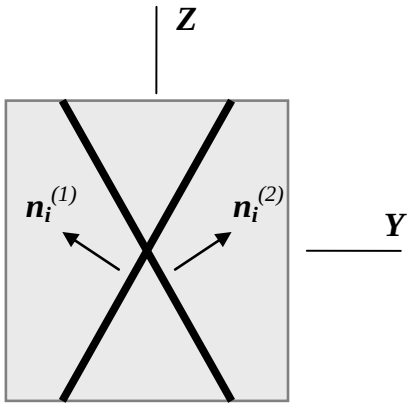

Fig. 6 Geometry of the problem

geometry of the problem is referred to the global coordinate system *XYZ*. The general formulation of the problem comprises two main aspects. The first one is related to specification of the conditions at failure for the joints. The second involves the description of localized deformation, after the onset of failure along a family of joints.

The conditions at failure for the family of joints are defined by the Coulomb criterion

$$F = \tau + \sigma_n \tan\varphi - c_0 = 0 \tag{16}$$

where, τ and σ_n are shear and normal components of the traction vector. Given the orientation of each family of joints, n_i, the failure criterion (16) can be checked to determine whether the conditions at failure have been reached.

The intact rock itself is considered as an elastic orthotropic or isotropic material, depending on its microstructure. The inception of localization is said to take place on one or both set of joints when the conditions at failure in Eq. (16) have been reached. The subsequent behaviour, after the inception of localized mode, is described by incorporating an averaging procedure, similar to that outlined in Section 2.2.

Referring to Fig. 6, the formulation of the problem incorporates the strain rate decomposition based on volume averaging

$$\dot{\varepsilon}_{ij}^{(0)} = \dot{\varepsilon}_{ij} - \upsilon^{(1)}\dot{\varepsilon}_{ij}^{(1)} - \upsilon^{(2)}\dot{\varepsilon}_{ij}^{(2)} \tag{17}$$

Here, the superscript (0) refers to the intact material outside the localization zone, the indexes (1) and (2) reference the material in the fractured zones and υ's represent the corresponding volume fractions. All quantities are referred to the global coordinate system, *XYZ*. The strain rate in the fractured zones may be defined in terms of a symmetric part of a dyadic product of n_i and the velocity discontinuities $\dot{g}_i$. Assuming that the predominant deformation mode for the weakness planes is the plastic deformation, i.e., $\dot{g}_i \approx \dot{g}_i^p$, we have

$$\dot{\varepsilon}_{ij}^{(1)} = \frac{1}{2h^{(1)}}(\dot{g}_i^{p(1)} n_j^{(1)} + \dot{g}_j^{p(1)} n_i^{(1)}); \quad \dot{\varepsilon}_{ij}^{(2)} = \frac{1}{2h^{(2)}}(\dot{g}_i^{p(2)} n_j^{(2)} + \dot{g}_j^{p(2)} n_i^{(2)}) \tag{18}$$

where $h^{(1)}$ and $h^{(2)}$ denote the thickness of the joint families (1) and (2), respectively.

The equilibrium requires that the traction $\dot{t}_i$ vector along the weakness planes remains continuous. Thus,

$$\dot{t}_i^{(1)} = \dot{\sigma}_{ij} n_j^{(1)}; \quad \dot{t}_i^{(2)} = \dot{\sigma}_{ij} n_j^{(2)} \tag{19}$$

Assume now the constitutive relations for all constituents take the general form

$$\dot{\varepsilon}_{ij}^{(0)} = C_{ijkl}\, \dot{\sigma}_{kl}; \quad \dot{g}_i^{p(1)} = K_{ij}^{(1)} \dot{t}_j^{(1)}; \quad \dot{g}_i^{p(2)} = K_{ij}^{(2)} \dot{t}_j^{(2)} \tag{20}$$

where C_{ijkl} is, in general, an orthotropic elastic compliance operator. Substituting the last two relations in Eq. (20) into Eq. (18), and taking into account Eq. (19) gives

$$\begin{aligned} \dot{\varepsilon}_{ij}^{(1)} &= \frac{1}{2h^{(1)}}(K_{ip}^{(1)} n_j^{(1)} n_k^{(1)} + K_{jp}^{(1)} n_i^{(1)} n_k^{(1)})\, \dot{\sigma}_{pk} \\ \dot{\varepsilon}_{ij}^{(2)} &= \frac{1}{2h^{(2)}}(K_{ip}^{(2)} n_j^{(2)} n_k^{(2)} + K_{jp}^{(2)} n_i^{(2)} n_k^{(2)})\, \dot{\sigma}_{pk} \end{aligned} \tag{21}$$

Thus, in view of the strain decomposition (18)

$$\begin{aligned} \dot{\varepsilon}_{ij} = [\, & C_{ijpk} + \frac{1}{2}\mu^{(1)}(K_{ip}^{(1)} n_j^{(1)} n_k^{(1)} + K_{jp}^{(1)} n_i^{(1)} n_k^{(1)}) + \\ & \frac{1}{2}\mu^{(2)}(K_{ip}^{(2)} n_j^{(2)} n_k^{(2)} + K_{jp}^{(2)} n_i^{(2)} n_k^{(2)})\,]\, \dot{\sigma}_{pk} \end{aligned} \tag{22}$$

The above expression represents the averaged constitutive relation which relates the macroscopic stress rates to the corresponding strain rates. In Eq. (22), $\mu^{(1)} = \upsilon^{(1)} / h^{(1)}$ and $\mu^{(2)} = \upsilon^{(2)} / h^{(2)}$ define the ratio of the area of the joint to the volume of the sample for joints (1) and (2), respectively. Thus both these parameters are, again, independent of *h*. It should be noted that since $\upsilon^{(1)} \ll \upsilon^{(0)} \wedge \upsilon^{(2)} \ll \upsilon^{(0)}$, the stress decomposition simplifies to $\dot{\sigma}_{ij} \approx \upsilon^{(0)} \dot{\sigma}_{ij}^{(0)} \approx \dot{\sigma}_{ij}^{(0)}$; the latter simplification was implemented in formulating the constitutive law above.

The description of the deformation process, viz. Eq. (22), requires the specification of the operator K_{ij}, which defines the properties of the material confined to the fracture zone. These properties have been described here by invoking a simple plasticity framework, which incorporates a strain-softening. The yield criterion has been assumed in a functional form consistent with representation (16), in which $c = c(\kappa)$ is the softening function and $\varphi = const.$ The strain-softening effects have been attributed to the norm of the plastic velocity discontinuity vector g_i^p

and the degradation function $c = c(\kappa)$ has been selected in a simple exponential form

$$c = c_0\, e^{-\mu\kappa}; \qquad \kappa = \int \sqrt{(\dot{g}_1^p)^2 + (\dot{g}_2^p)^2 + (\dot{g}_3^p)^2}\, dt \tag{23}$$

where c_o is the shear strength of the joint at $\sigma_n = 0$, Eq. (16), and μ represents a material constant. Given the above expression, the operator K_{ij} can be established following standard plasticity formalism.

(ii) Stability indicator

Based on the work reported by Pietruszczak and Oulapour (1999), the stability criterion is derived by considering a perturbation in the displacement field and employing the differential equations of motion. The sufficient condition for stability is defined by imposing the requirement of the existence of the solution for a free vibration problem associated with the perturbation in velocities. This procedure leads to definition of a stability indicator that is expressed in terms of the second rate of work as

$$SI = \frac{\int_V \dot{\boldsymbol{\varepsilon}}^T \dot{\boldsymbol{\sigma}}\, dV}{\int_V \dot{\boldsymbol{\varepsilon}}^T \dot{\boldsymbol{\sigma}}^e\, dV} = \frac{\int_V \dot{\boldsymbol{\varepsilon}}^T [D] \dot{\boldsymbol{\varepsilon}}\, dV}{\int_V \dot{\boldsymbol{\varepsilon}}^T [D^e] \dot{\boldsymbol{\varepsilon}}\, dV}; \qquad \textit{stable system}: \; 1 \geq SI > 0 \tag{24}$$

where $[D^e], [D]$ represent the elastic and elastoplastic stiffness operators, respectively, $\dot{\boldsymbol{\sigma}}$ is the actual stress rate, $\dot{\boldsymbol{\sigma}}^e$ is the elastic stress increment, and the integration is carried out over the entire domain. It should be noted that in elastic range the value of *SI* remains equal to one, while beyond that limit it gradually decreases until, at the onset of global instability, it becomes equal to zero.

(iii) Numerical results

Finite element discretization of the spent fuel pool and the rock foundation, using 8-noded solid elements, is depicted in Fig. 7. The figure shows, once again, the regions within the structure with different ultimate free expansions due to AAR. The values range from $20 - 120 \times 10^{-6}$/yr. The basic material parameters for concrete have been assumed as follows:

Table 2 Rock properties

Foundation	Material Property No.	Young's Modulus E(GPa)	Shear Modulus G (GPa)	Joint tension Cut-off σ_o(MPa)	Joint Cohension C_o (MPa)	Joint friction Angle Φ(°)	Joint 1 Orientation Ψ_1(°)	Joint 2 Orientation Ψ_2(°)
Rock	MP1	2.25	0.94	0.1	0.2	33.5	70	110
	MP2	7.7	3.21	0.65	1.3	41.5	70	110
	MP3	28.65	11.94	3.8	7.6	47	70	110
Connection	MP4	7.7	3.21	0.01	0.02	45	5	175
	MP5	7.7	3.21	0.01	0.02	45	85	95

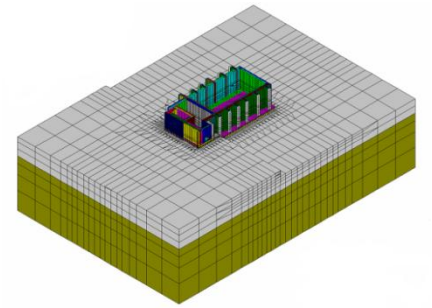

Fig. 7 FE discretization of the structure and the rock foundation

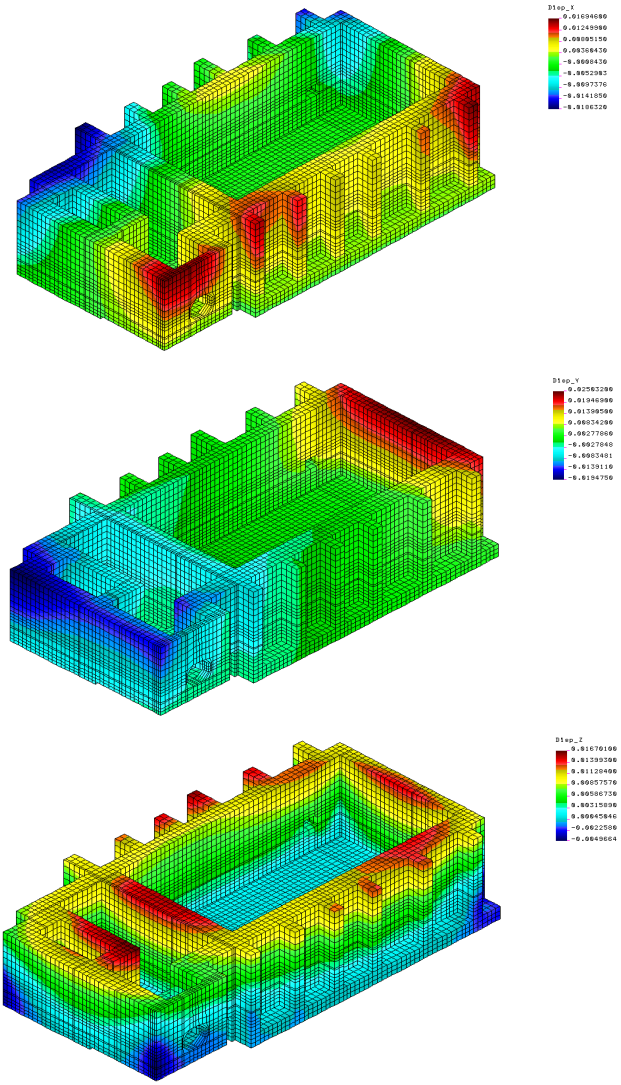

Fig. 8 Displacement distribution in x, y, and z directions after 50 years of AAR

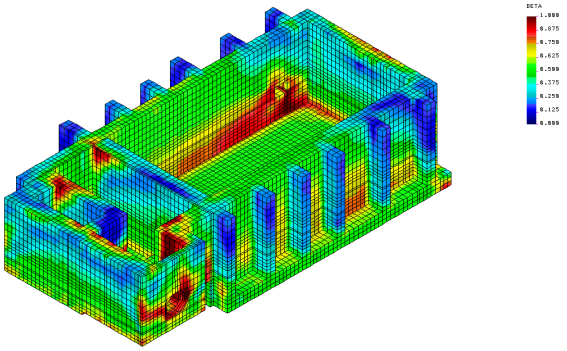

(a)

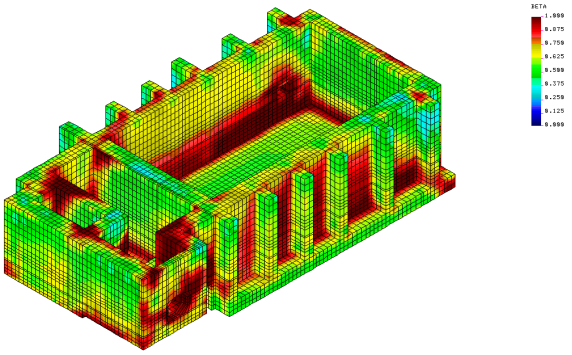

(b)

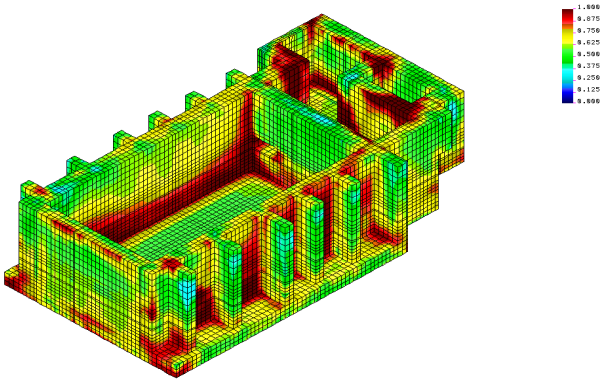

(c)

Fig. 9 Distribution of damage factor, β, after (a) 15 years, (b) and (c) 50 years of AAR (different views)

$$E_0 = 26.5\,\text{GPa}, \quad \nu_0 = 0.18, \quad f_c = 27\,\text{MPa}, \quad f_t = 2.07\,\text{MPa}$$

For steel, the following properties were assigned: $E_s = 200\,\text{GPa}$, $\nu_s = 0.3$, uniaxial yield limit $\sigma_y = 400\,\text{MPa}$. The values of material parameters governing the kinetics of the reaction and the rate of degradation were taken as

$$\gamma = 0.000293\ (1/month)\ ;\ B_1 = 0.3\ ;\ B_2 = 1\ ;\ B_3 = 0.85\ ;\ A_1 = 8.3$$

The properties of the intact rock and the joints are shown in Table 2, in which MP2 and MP3 refers to the grey and green parts, respectively (see Fig. 7). Note that the spacing of the joints is small compared to the dimensions of the problem, so that the averaging procedure employed in 3.2(*ii*) is used throughout the solution domain. The bedrock is significantly weathered close to the surface, which results in low values of elastic moduli and strength properties (MP1). For describing the interface, the softening parameter μ was taken as 100m^{-1}.

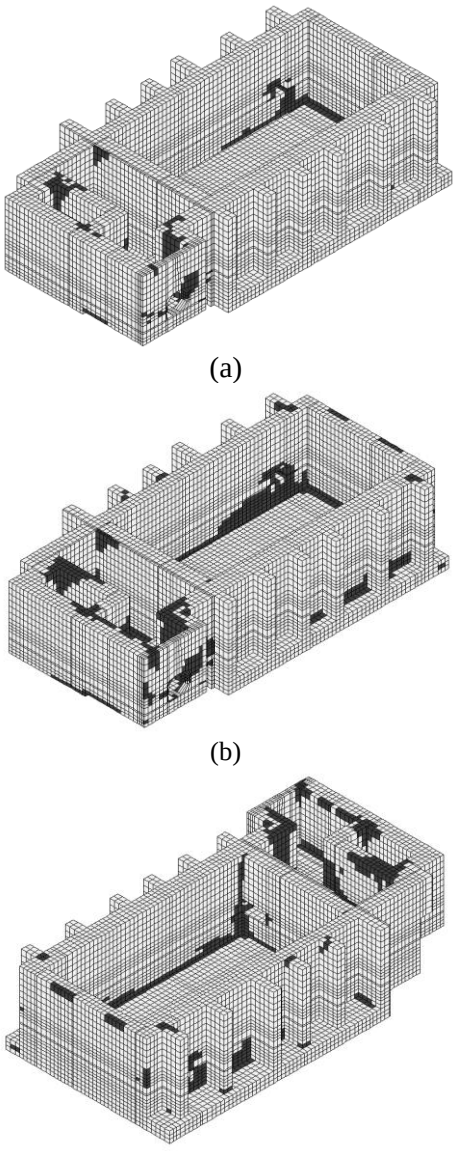

(a)

(b)

(c)

Fig. 10 Damaged regions (marked in dark grey) after (a) 15 years, (b) and (c) 50years of AAR

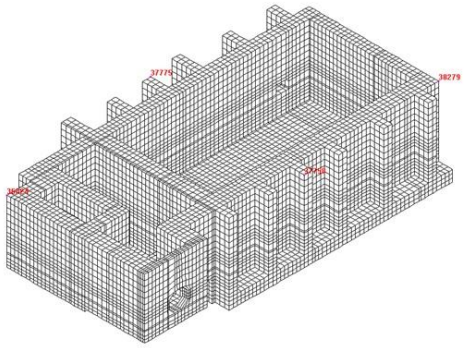

Fig. 11 Location of the selected nodes

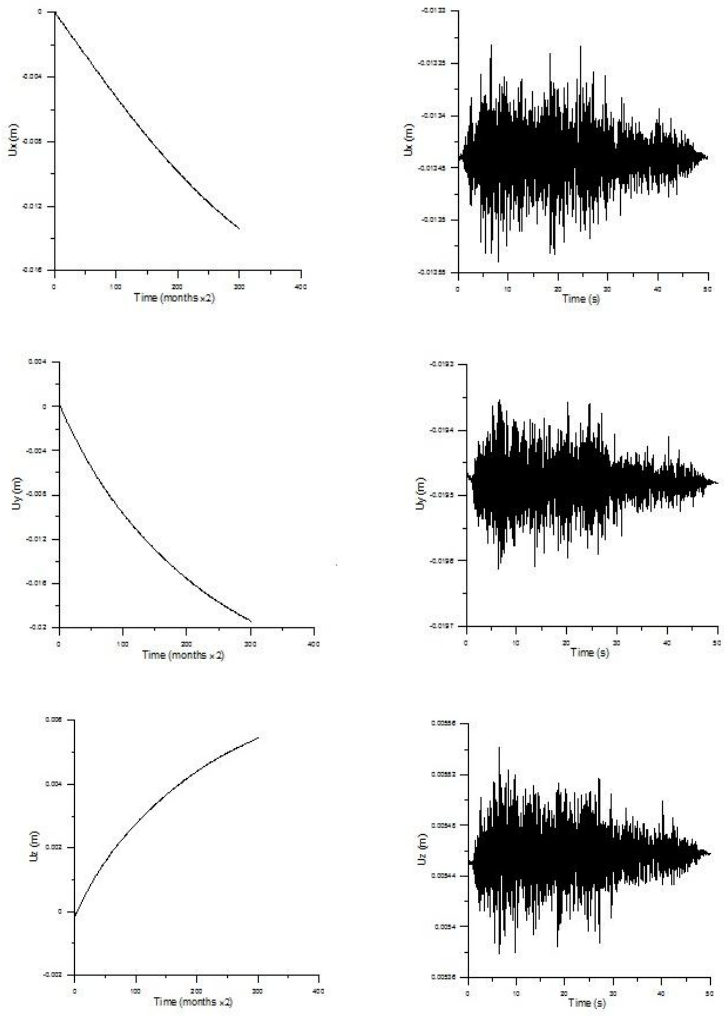

Fig. 12 Displacement histories for node #36824, under self-weight + AAR and during seismic excitation

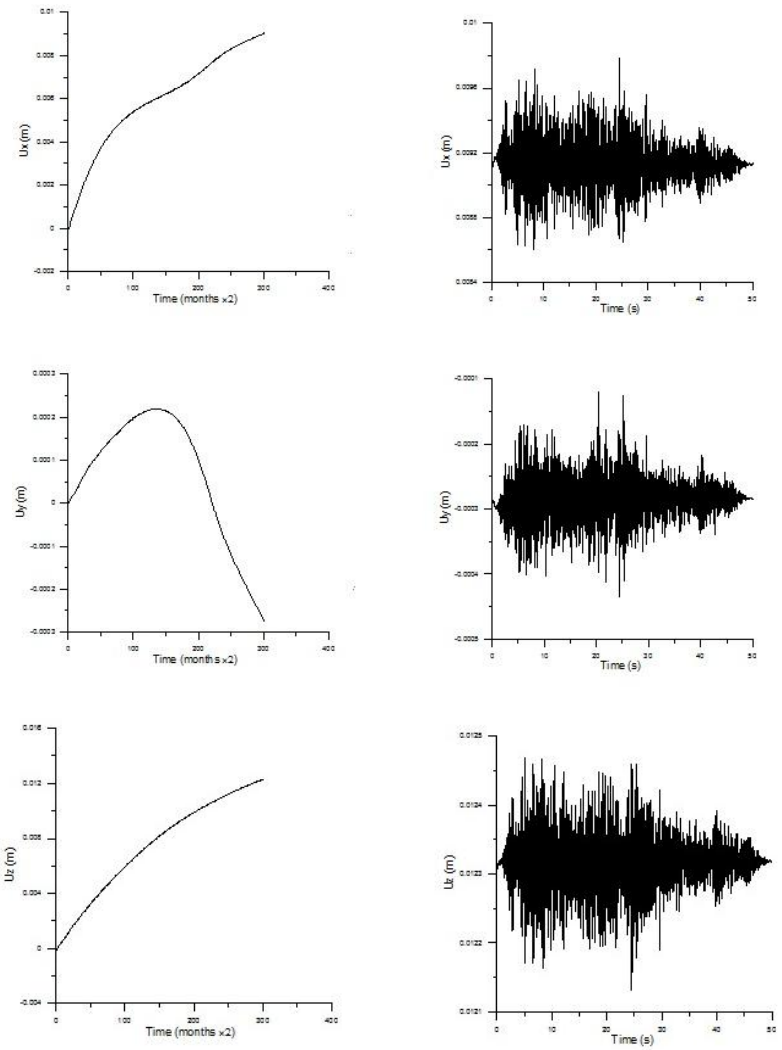

Fig. 13 Displacement histories for node #37758, under self-weight + AAR and during seismic excitation

The results of the analysis for the structure subjected to a continuing AAR as well as a seismic load, typical of the region, are presented in the set of figures below. Fig. 8 shows the displacements in three different directions, *x*, *y*, and *z* after 50 years of AAR. The evolution of the distribution of damage factor *ß* is shown in Fig. 9. The corresponding cracked regions are shown in Fig. 10.

The displacement histories due to self-weight and AAR, for some arbitrarily selected nodes (viz. Fig. 11), are depicted in Figs. 12-13. The evolution of displacements corresponding to the seismic event is also shown in the same figures. Finally, it should be mentioned that the distribution of damage factor during the seismic activity is virtually the same as that corresponding to 50 years of AAR, as shown in Fig. 9. This indicates that the predominant source of damage is the 50 years of the continuing AAR.

Fig. 14 shows the evolution of damaged zone (marked in dark grey) in rock foundation under

continuing AAR. The damaged zones are in close proximity to the area where the pool is placed on the foundation. Fig. 15 shows the longitudinal and cross sectional views of the damaged zones within the rock mass, after 40 months, and 50 years of AAR. The figure shows that the damaged zone due to the continuing AAR gradually propagates into the rock mass. Finally, the evolution of stability indicator for rock foundation under continuing AAR and seismic load is shown in Figs. 16 and 17, respectively.

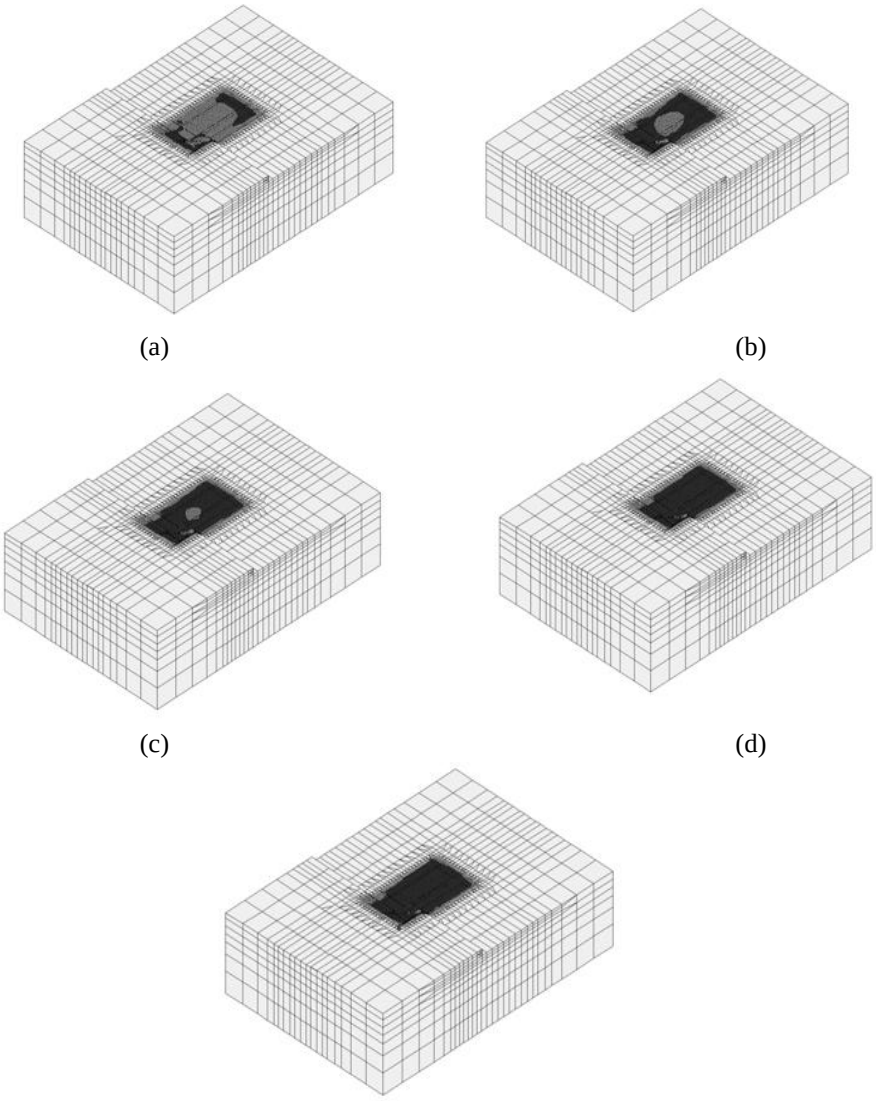

Fig. 14 Evolution of damaged zone (marked in dark grey) in rock foundation, after (a) 40 months, (b) 5 years, (c) 80 months, (d) 10 years, and (e) 50 years of AAR

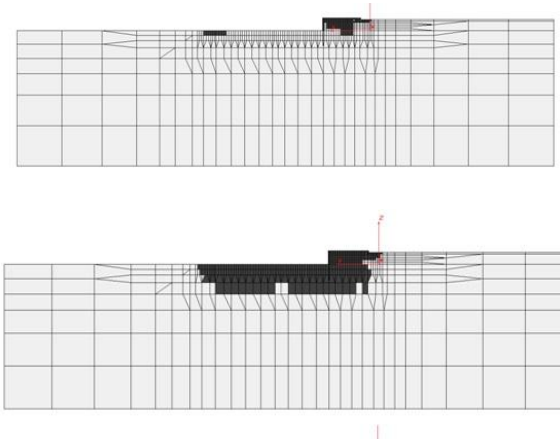

(a) Longitudinal sections

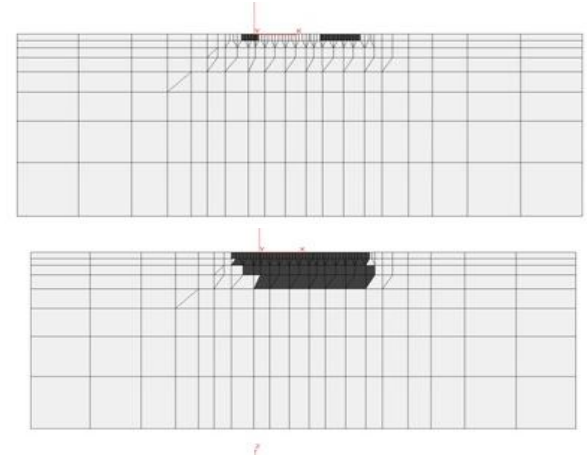

(b) Cross sections

Fig. 15 Fig. 15 Longitudinal and cross sectional views of evolution of damaged zone (marked in dark grey) in the rock mass; comparing 40 months, and 50 years of AAR

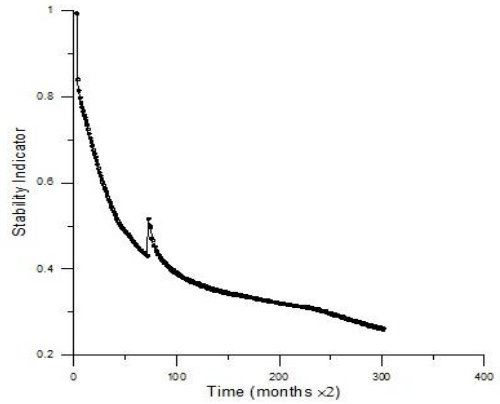

Fig. 16 Evolution of stability indicator during AAR for rock foundation

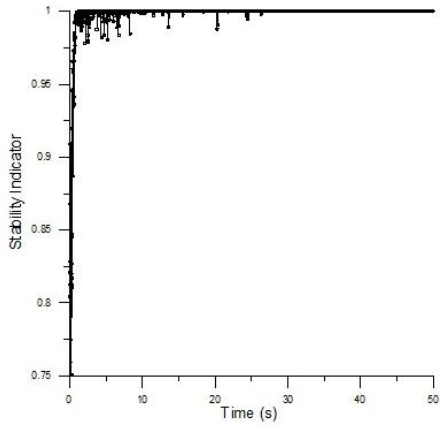

Fig. 17 Time history of the stability indicator for rock foundation under seismic load

4. Conclusions

A meso-scale approach has been outlined for describing the chemo-mechanical interaction in reinforced concrete. The formulation has been incorporated in a finite element code to examine the mechanical behaviour of some reinforced concrete structures in nuclear power facilities located in Quebec, Canada. First, the response of a containment structure under self-weight, post-tensioning, and continuing AAR was examined. A formation of some zones of micro/macro-cracking was predicted in the walls of the containment building over 45 years of reaction. Subsequently, finite element simulations were carried out to analyze the reinforced concrete fuel storage pool of G2. The numerical simulation involved the prediction of inelastic response of the pool founded on jointed rock mass under 50 years of continuing AAR and seismic load typical for the region. The analysis incorporated non-linear elasto-plastic properties of the foundation. The results indicate the presence of macrockracking along the walls of the spent fuel pool, which is consistent with the in-situ observation.

In general, the obtained results are in agreement with findings based on numerous in-situ measurements as well as conclusions in several inspection reports during the period from the plant construction in 1976 up until today (2011). The predictions for the subsequent 25 years, i.e. till plant decommissioning (around 2035), are currently being incorporated in the Aging Management Program (AMP) of the concrete containment structure developed for the G-2 NPP. The primary objective of the AMP is to ensure that the requirements of CSA Standard N278.7-08 are met and will continue to be met for the period through which the structure will remain operational.

References

Bažant, Z.P., and Steffens, A. (2000), "Mathematical model for kinetics of alkali-silica reaction in concrete", *Cem. Concr. Res.*, **30**, 419-428.

Bažant, Z.P., Zi, G., and Meyer, C.H. (2000), "Fracture mechanics of ASR in concretes with waste glass particles of different sizes", *J. Engng Mech., ASCE*, **126**, 226-232.

Broekmans, M. and Wigum, B.J. – Editors (2008), Proceedings of the 13th Intern. Conf. on Alkali-Aggregate Reaction in Concrete, Trondheim, Norway.

Canadian Journal of Civil Engineering (2000), Special issue on alkali-reactivity in Canada, **2,** 167-388.

Capra, B. and Bournazel, J.P. (1998), "Modeling of induced mechanical effects of alkali-aggregate reactions", *Cem. Concr. Res*., **28**, 251-260.

Dhir, R.K., Dyer, T.D. and Tang, M.C. (2009), "Alkali-silica reaction in concrete containing glass", *Mat. Structures*, **42**, 1451-1462.

Gocevski, V. (2003), "Centrale nucléaire de Gentilly-2; analyse du comportement du bâtiment du réacteur", Volume 1 du Rapport Final, Hydro-Québec TAYAA-12242-001.

Gocevski, V. (2010), "Gentilly 2 NPP - concrete aging effects on long term pre-stress losses and propagation of concrete cracking due to pressure testing", *International Symposium, Fontevraud-7, SFEN French Nuclear Energy Society,* Avignon, France, Paper A158-T10, 26-30.

Grimal, E., Sellier, A., Le Pape, Y. and Bourdarot, E. (2008), "Creep, shrinkage and anisotropic damage in alkali-aggregate reaction swelling mechanism – Part I : A constitutive model ", *ACI Mater. Journ.* **105**, 227-235.

Herrador, M., Martinez-Abella, F. and Dopico J.R.R. (2008), "Experimental evaluation of expansive behaviour of an old-aged ASR-affected dam concrete: methodology and application", *Mat. Structures*, **41**, 173-188.

Hill, R. (1963), "Elastic properties of reinforced solids: some theoretical properties", *J. Mech. Phys. Solids*, **11**, 357-372.

Larive, C. (1998), "Apports combinés de l'expérimentation et de la modélisation à la comprehension de l'alcali reaction et de ses effets mécaniques", *Momograph LPC*., OA 28, Laboratoires des Ponts et Chaussées, Paris, France.

Multon, S. and Toutlemonde, F. (2006), "Effect of applied stresses on alkali-silica reaction-induced expansions", *Cem. Concr.Res.*, **36**, 912-920.

Pietruszczak, S. (1996), "On the mechanical behaviour of concrete subjected to alkali – aggregate reaction", *Comput. Struct.*, **58**, 1093-1097.

Pietruszczak, S. and Gocevski, V. (2002), "On rehabilitation of concrete structures affected by alkali-silica reaction", *Int. J. Comp. Civil Struct. Eng*., **1**, 182-197.

Pietruszczak, S., Jiang, J. and Mirza, F.A. (1988), "An elastoplastic constitutive model for concrete", *Int. J. Solids Struct*., **24**, 70-722.

Pietruszczak S. and Oulapour M. (1999), "Assessment of dynamic stability of foundations on saturated sandy soils", *Journal Geotech. Eng., ASCE,* **125**, 576-582.

Pietruszczak, S. and Winnicki, A. (2003), "Constitutive model for concrete with embedded sets of reinforcement", *J. Eng. Mech., ASCE*, **129**, 725-738.

Poyet, S., Sellier, A., Capra, B., Foray, G., Torrenti, J.M., Cognon, H. and Bourdarot, E. (2006), "Influence of water on alkali-silica reaction: Experimental study and numerical simulations", *J. Mat. Civil Eng.*, **18**, 588-596.

Poyet, S., Sellier, A., Capra, B., Foray, G., Torrenti, J.M., Cognon, H. and Bourdarot, E. (2007), "Chemical modeling of alkali-silica reaction: Influence of the reactive aggregate size distribution", *Mat. Struct.*, **40**, 229-239.

Tang, M. and Deng, M. (2004), Proceedings of the 12th Intern. Conf. on Alkali-Aggregate Reaction in Concrete, Beijing, China

Rivard, P., Berube, M.A. and Ollivier, J.P. (2007), "Decrease of pore solution alkalinity in concrete tested for alkali-silica reaction", *Mat. Struct.*, **40**, 909-921.

Saouma, V. and Perotti, L. (2006), "Constitutive model for alkali-aggregate reaction", *ACI Mat. J*., **103,** 194 -202.

Sellier, A., Bourdartt, E., Multon, S., Cyr, M. and Grimal, E. (2009), "Combination of structural monitoring and laboratory tests for assessment of alkali-aggregate reaction swelling: Application to gate structure dam", *ACI Mat. J*., **106**, 281-290.

Steffens, A., Kefei, L. and Coussy, O. (2003), "Aging approach to water effect on alkali-silica reaction degradation of structures", *J. Eng. Mech., ASCE*, **129**, 50-59.
Ulm, F.J., Coussy, O., Kefei, L. and Larive, C. (2000), "Thermo-chemo-mechanics of ASR expansion in concrete structures", *J. Eng. Mech., ASCE*, **126**, 233-242.
Winnicki, A. and Pietruszczak, S. (2008), "On mechanical degradation of reinforced concrete affected by alkali-silica reaction", *J. Eng. Mech., ASCE*, **134**, 611-627.

CC